

# Three-dimensional random dielectric colloid metamaterial with giant isotropic optical activity

Viktar S. Asadchy<sup>1,\*</sup>, Cheng Guo<sup>2</sup>, Ihar A. Faniayeu<sup>3</sup>, and Shanhui Fan<sup>1†</sup>

<sup>1</sup>*Ginzton Laboratory and Department of Electrical Engineering,  
Stanford University, Stanford, California 94305, USA*

<sup>2</sup>*Department of Applied Physics, Stanford University, Stanford, California 94305, USA*

<sup>3</sup>*Department of Physics, University of Gothenburg, 412 96 Gothenburg, Sweden*

Motivated by the theoretical observation that isotropic chirality can exist even in completely random systems, we design a dielectric metamaterial consisting of a random colloid of meta-atoms, which exhibits unprecedentedly high isotropic optical activity. Each meta-atom is composed of a helically arranged cluster of silicon nanospheres. Such clusters can be fabricated by large-scale DNA self-assembly techniques. We demonstrate that the use of a high concentration of the meta-atoms in the colloid provides significant suppressions of incoherent scattering losses. As a result, our system shows three orders of magnitude improvement of isotropic optical activity as compared with the previous metamaterial designs. Our work highlights the significant potential of completely random system, which are commonly produced in colloidal sciences, for applications as metamaterials towards novel photonic effects and devices.

## I. MAIN TEXT

The development of metamaterials opens numerous new opportunities for manipulating electromagnetic waves. Most metamaterial structures consist of regular array of meta-atoms [1]. As an alternative, one may wonder whether or how one can achieve non-trivial metamaterial functionalities in complete random or disordered systems. This is important from a fundamental perspective in the context of recent efforts in exploring the effects of disorders in photonic systems [2–7]. It is also of significance from a practical point of view, since many large-scale fabrication techniques, such as self-assembly techniques, readily produce random array of meta-atoms [8–13].

For a linear metamaterial consisting of an completely random array of meta-atoms, after homogenization, its electromagnetic properties can be described by an effective medium with the following constitutive relations [14, p. 28]:

$$\begin{aligned}\mathbf{D} &= \varepsilon \cdot \mathbf{E} + \xi \cdot \mathbf{H}, \\ \mathbf{B} &= \mu \cdot \mathbf{H} + \zeta \cdot \mathbf{E}.\end{aligned}\tag{1}$$

Here  $\mathbf{D}$ ,  $\mathbf{B}$ ,  $\mathbf{E}$ , and  $\mathbf{H}$  are the electric and magnetic displacement vectors and fields,  $\varepsilon$  and  $\mu$  are the permittivity and permeability tensors, respectively, and  $\xi$  and  $\zeta$  are the bianisotropic tensors. If one further assumes that the effective medium is lossless, then  $\xi = \zeta^\dagger$  [14, § 2.7]. Since the array is completely random, the effective medium must be rotationally invariant. Consequently,  $\varepsilon$ ,  $\mu$  and  $\xi$  must all be scalar. The imaginary part of  $\xi$  describes effect of isotropic chirality (natural optical activity), which

is a reciprocal effect, while the real part of  $\xi$  describes the effect of isotropic magneto-electric coupling, which is a non-reciprocal effect. Therefore, one should be able to observe isotropic chirality or isotropic magneto-electric coupling even in a system that is completely random.

Motivated by the theoretical considerations above, in this Letter, we introduce a dielectric metamaterial consisting of a random colloid of specifically designed silicon nanoclusters in order to achieve giant isotropic chirality. We demonstrate that due to the absence of absorption, the concentration of the nanoclusters in the colloid can be very high, which, in turn, provides a significant suppression of incoherent scatterings. Our metamaterial colloid exhibits isotropic chirality that is three orders of magnitude higher than those of previously reported isotropic chiral materials. Moreover, we demonstrate that similar superiority is achieved in terms of the figure of merit given by the ratio of the chirality parameter and the average extinction coefficient.

Chirality phenomenon, first observed more than two centuries ago [15], is of current importance for a diversity of applications such as in organic and inorganic chemistry, pharmaceutical engineering, optical communications, displays, spectroscopy, and sensors [16–19]. The chiral effects in naturally occurring materials are relatively weak. Therefore, there is significant recent interest in designing metamaterials [1, 20–27] and colloids [11–13, 25, 28–30] with enhanced chiral response. In particular, there is an extensive literature on the chiral properties of metasurfaces [31–34]. The chiral response of a three-dimensional metamaterial, however, can be qualitatively different. In particular, isotropic chiral response, where the same chiral effects occur independently of the directions of light propagation, is a three-dimensional effect that is difficult to achieve with metasurfaces. Such an isotropic chiral response is potentially important for topological photonics [35, 36] and stereochemistry [18, 37]. Moreover, isotropic chiral materials provide an attractive route towards achieving

\* asadchy@stanford.edu

† shanhui@stanford.edu

the phenomenon of negative refraction in bulk [24, 38]. In the optical frequency range, the existing designs of three-dimensional chiral metamaterials rely upon metallic structures with complex geometries [1, 25–27]. The use of metal introduces significant inherent loss, whereas the use of complex geometries represents major challenges for three-dimensional nanofabrication. Our proposed chiral metamaterial colloid overcomes all the above mentioned drawbacks.

In an isotropic chiral material, the right (RCP) and left (LCP) circularly polarized light are eigenstates for all propagation directions. The chirality parameter of a material is defined as  $\kappa = (n_- - n_+)/2$ , where  $n_+$  and  $n_-$  are the refractive indices for right and left circularly polarized light, respectively [19]. The isotropic chirality results in the optical rotation  $\Delta\theta$  and the circular dichroism  $\eta$  for linearly polarized waves propagating over distance  $L$  in the material, which is expressed as  $\Delta\theta + i\eta = \omega\kappa L/c$  [16, § 5.2]. Time harmonic oscillations in the form  $e^{-i\omega t}$  are assumed throughout the paper. For a metamaterial, the chirality parameter is nonzero only when the constituent meta-atoms have no mirror symmetry. For low-concentration colloids, the macroscopic chirality parameter and the properties of the individual meta-atoms are related by [14, § 2.10.1]

$$\kappa = \frac{N}{3} \text{tr}\{\bar{\bar{\alpha}}_{\text{em}}\}, \quad (2)$$

where  $N$  is the volume concentration of the constituent meta-atoms in the colloid and  $\bar{\bar{\alpha}}_{\text{em}}$  is the magnetoelectric polarizability tensor of each meta-atom. This relation is equivalent to the Rosenfeld equation in chemistry literature [16, Eq. 5.2.2]. For high constituent concentrations, the chirality parameter is obtained using the Maxwell Garnett mixing rule starting from (2) [14, § 7.2.2]. Relation (2) is rotationally invariant since the trace of a matrix does not change under rotations.

As is seen from (2), when choosing the constituent meta-atom for our colloid, we need to maximize the trace of its magnetoelectric polarizability tensor  $\bar{\bar{\alpha}}_{\text{em}}$ . Next, we suggest a simple extraction technique of this trace for an arbitrary meta-atom. The technique is based on a previously proposed method based on the far-field scattered fields [39]. Consider an arbitrary meta-atom in free space. First, we illuminate it with RCP or LCP monochromatic light with electric field amplitude  $\mathbf{E}_{\pm} = (\mp i; 0; 1)^T E_0$  and wave vector  $\mathbf{k} = -\omega/c \hat{\mathbf{y}}$ , as shown with orange arrows in Fig. 1. The upper and bottom signs correspond to the right and left circular polarizations, respectively. The incident magnetic field is  $\mathbf{H}_{\pm} = \mathbf{k} \times \mathbf{E}_{\pm} / (\omega\mu_0)$ . Within the dipolar approximation, the induced electric and magnetic dipole moments in the meta-atom due to the incident light read

$$\begin{aligned} \mathbf{p}_{\pm} &= \varepsilon_0 \bar{\bar{\alpha}}_{\text{ee}} \cdot \mathbf{E}_{\pm} + \frac{i}{c} \bar{\bar{\alpha}}_{\text{em}} \cdot \mathbf{H}_{\pm}, \\ \mathbf{m}_{\pm} &= \mu_0 \bar{\bar{\alpha}}_{\text{mm}} \cdot \mathbf{H}_{\pm} + \frac{i}{c} \bar{\bar{\alpha}}_{\text{me}} \cdot \mathbf{E}_{\pm}, \end{aligned} \quad (3)$$

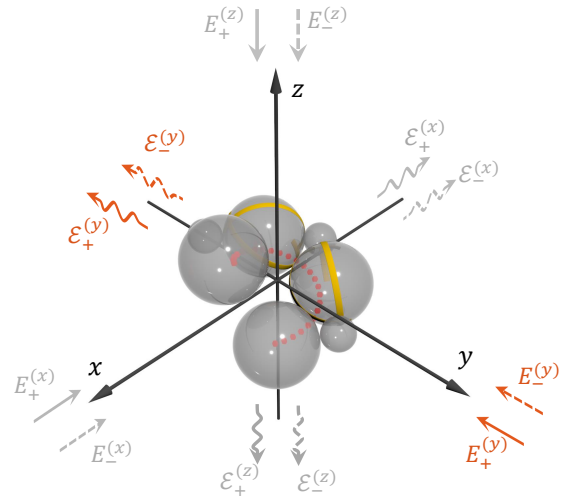


FIG. 1: Designer dielectric chiral meta-atom assembled as a cluster of crystalline silicon nanospheres. The nanospheres are DNA-coated and hybridized by DNA origami belts (shown as yellow strips) to one another, forming a three-dimensional helical shape (shown by red dots). The straight and curly arrows denote the directions of the incident and forward-scattered light, respectively. The plus and minus subscripts stand for RCP and LCP light, respectively. Six measurements of the forward-scattered light with two polarizations and along three illumination directions enable accurate and unambiguous calculation of the intrinsic (isotropic) chiral properties of the meta-atom.

where  $\bar{\bar{\alpha}}_{\text{ee}} = \bar{\bar{\alpha}}_{\text{ee}}^T$  and  $\bar{\bar{\alpha}}_{\text{mm}} = \bar{\bar{\alpha}}_{\text{mm}}^T$  are the electric and magnetic polarizability tensors, and  $\bar{\bar{\alpha}}_{\text{me}} = -\bar{\bar{\alpha}}_{\text{em}}^T$  for reciprocal meta-atoms [14, § 3.3.1]. All the polarizability tensors in (3) have units of volume. One can then find the scattered field by the meta-atom in the forward direction  $\mathbf{n} = -\hat{\mathbf{y}}$  at a distance  $r$  [40, p. 457]:

$$\mathbf{E}_{\text{sc}\pm} = \frac{\omega^2 e^{i\omega r/c}}{4\pi\varepsilon_0 r c^2} \left[ (\mathbf{n} \times \mathbf{p}_{\pm}) \times \mathbf{n} - \frac{\mathbf{n} \times \mathbf{m}_{\pm}}{c\mu_0} \right]. \quad (4)$$

Here  $\mathbf{E}_{\text{sc}+}$  and  $\mathbf{E}_{\text{sc}-}$  represent scattered fields when the meta-atom was illuminated by RCP (first scenario) and LCP (second scenario) light, respectively. Next, expressing the right circular polarization component of the scattered field in the first scenario as  $\mathcal{E}_+ = (\hat{\mathbf{z}} + i\hat{\mathbf{x}}) \cdot \mathbf{E}_{\text{sc}+}/2$  and the left circular polarization component in the second scenario as  $\mathcal{E}_- = (\hat{\mathbf{z}} - i\hat{\mathbf{x}}) \cdot \mathbf{E}_{\text{sc}-}/2$ , we obtain the linear relation for the magnetoelectric polarizability components:

$$\frac{2\pi r c^2}{\omega^2 e^{i\omega r/c}} (\mathcal{E}_+^{(y)} - \mathcal{E}_-^{(y)}) = (\alpha_{\text{em}}^{xx} + \alpha_{\text{em}}^{zz}) E_0, \quad (5)$$

where the superscript  $y$  was added to indicate that the incident light in this scenario propagates along the  $y$  axis in the given basis. Note that in this relation, the only unknown is the sum of the polarizability components (the scattered fields can be calculated from full-wave simulations).

Repeating the same procedure for two other sets of illuminations of the meta-atom along the  $-\hat{x}$  and  $-\hat{z}$  directions (shown with grey arrows in Fig. 1) and summing up the results in the form of (5), one can finally arrive at the following expression:

$$\text{tr}\{\bar{\alpha}_{\text{em}}\} = \frac{\pi r c^2}{\omega^2 E_0 e^{i\omega r/c}} \sum_{m=x,y,z} \left( \mathcal{E}_+^{(m)} - \mathcal{E}_-^{(m)} \right). \quad (6)$$

This expression allows simple calculation of the trace of the magnetoelectric tensor of an unknown meta-atom from six scattering calculations. As one can see, the trace as well as optical activity (according to relation (2)) are maximized when the meta-atom exhibits the highest contrast in forward scattering of incident RCP and LCP light for the three orthogonal directions. It is worth mentioning that the derived expression (6) to some extent resembles the conventional dimensionless circular intensity difference parameter defined as  $\Delta = (I_+ - I_-)/(I_+ + I_-)$  [16, p. 162], where  $I_+$  and  $I_-$  are the scattering intensities of the meta-atom excited by the incident RCP and LCP light, respectively. Our relation has an important advantage. It uniquely characterizes the magnetoelectric polarizability and isotropic chirality parameter, while parameter  $\Delta$  additionally depends on electric dipolar and quadrupole polarizability contributions.

Next, we design the constituent meta-atom in the form of a cluster of dielectric nanospheres. In order to maximize the interaction between the meta-atoms and incident light, we need to use high-permittivity dielectric. For the chosen operational frequency of 400 THz ( $\lambda_0 = 750$  nm wavelength in vacuum or  $\lambda = 564$  nm in water where the meta-atoms are dispersed), a good candidate is crystalline silicon [41, 42]. Fabrication of both crystalline and amorphous silicon nanosphere colloids have been demonstrated in the literature [43–45]. The nanospheres in the colloid can be coated by DNA origami belts and hybridized to form a cluster with the desired chiral shape, as was demonstrated recently in [46]. Some alternative fabrication techniques for such a colloid metamaterial can be found in [47–53]. We choose the maximum size of the cluster meta-atom  $D_{\text{max}} = 130$  nm so that it remains subwavelength in water at wavelength  $\lambda = 564$  nm. Such choice, although not unique, was made in order to avoid generation of higher multipoles in the meta-atoms and diffraction effects, as well as to have the possibility of strong suppression of light scattering in the colloid metamaterial, as discussed below. With such a choice of sizes, the designed meta-atom is nonresonant: The first Mie resonance for a quasispherical nanoparticle at the chosen operating frequency occurs when its size is  $D_{\text{Mie}} \approx \lambda_0/n_{\text{Si}} = 202$  nm [54], which is twice larger than our chosen size  $D_{\text{max}}$ .

Using the expression (6) and calculating the six scattered far-fields  $\mathcal{E}_+$  and  $\mathcal{E}_-$  via ANSYS HFSS (a finite element method solver), we have found that the largest value of the trace of  $\bar{\alpha}_{\text{em}}$  tensor is achieved for a helically-shaped cluster of nanospheres. The designed chiral meta-atom is shown in Fig. 1 and consists of four larger

$\text{tr}\{\bar{\alpha}_{\text{ee}}\}/3$ [m <sup>3</sup> ]	$\text{tr}\{\bar{\alpha}_{\text{mm}}\}/3$ [m <sup>3</sup> ]	$\text{tr}\{\bar{\alpha}_{\text{em}}\}/3$ [m <sup>3</sup> ]
$(8.3 + i0.3) \cdot 10^{-22}$	$(5.4 + i0.3) \cdot 10^{-23}$	$(-8.0 + i0.2) \cdot 10^{-25}$

TABLE I: Dipolar polarizabilities of the designer dielectric meta-atom shown in Fig. 1 averaged over all orientations at the operational frequency of 400 THz.

nanospheres with diameters  $D = 52$  nm and three smaller nanospheres with diameters  $d = 20$  nm. Note that for simplifying fabrication, the three smaller nanospheres could be omitted, which would decrease the trace of  $\bar{\alpha}_{\text{em}}$  by approximately half. An imaginary line drawn through the centers of the larger nanospheres forms a helical trajectory with pitch of 58 nm and diameter of 66 nm (the neighbouring nanospheres are touching one another and the centers of the two outermost spheres are at the ends of the helical trajectory), as shown by the red dotted line in the figure. Each smaller nanosphere touches two larger ones such that a plane drawn through their centers (one smaller and two larger nanospheres) passes through the origin of the chosen coordinate system (see Fig. 1). Table (I) summarizes the traces of the dipolar electric, magnetic, and magnetoelectric polarizability tensors extracted using (6) and technique reported in [55]. As is seen, the largest isotropic response arises from the electric dipole excitation, exceeding by one or several orders of magnitude those of the magnetic dipole excitation and magnetoelectric coupling. The imaginary part of the trace of the polarizability takes into account both the scattering of light away from the direction of incidence, which becomes the incoherent scattering loss for the random metamaterial, as well as material absorption loss since the operating frequency is above the band gap of crystalline silicon. For the proposed meta-atom, the scattering loss dominates over the absorption loss by two orders of magnitude. Additionally, we have analyzed the trace of  $\bar{\alpha}_{\text{em}}$  tensor of a pyramidal cluster of nanospheres. It exhibits significantly smaller value, which is in agreement with the results in [11].

Next, we study optical response of the random distribution of the designed dielectric constituent meta-atoms, as shown in Fig. 1, dissolved in water. From (2), since the strength of the isotropic chirality parameter increases as the volume concentration  $N$  increases, we are interested in the regime with the high volume concentration. As a dimensionless measure of the volume concentration, we define  $N_V = NV_{\text{circ}}$ , where  $V_{\text{circ}}$  is the volume of the sphere circumscribed around the meta-atom shown in Fig. 1. For given volume concentration, we analytically calculate the relative permittivity  $\bar{\epsilon}$ , permeability  $\bar{\mu}$ , and chirality parameter  $\bar{\kappa}$  of the metamaterial using the Maxwell Garnett mixing rule [14, § 7.2.2], whose applicability is not limited to low concentrations, instead of Eq. (2). Effective refractive indices for RCP and LCP light propagating in the colloid metamaterial are expressed as  $n_{\pm} = \sqrt{\bar{\epsilon}\bar{\mu}} \mp \bar{\kappa}$  [56, § 2.2.1]. In order

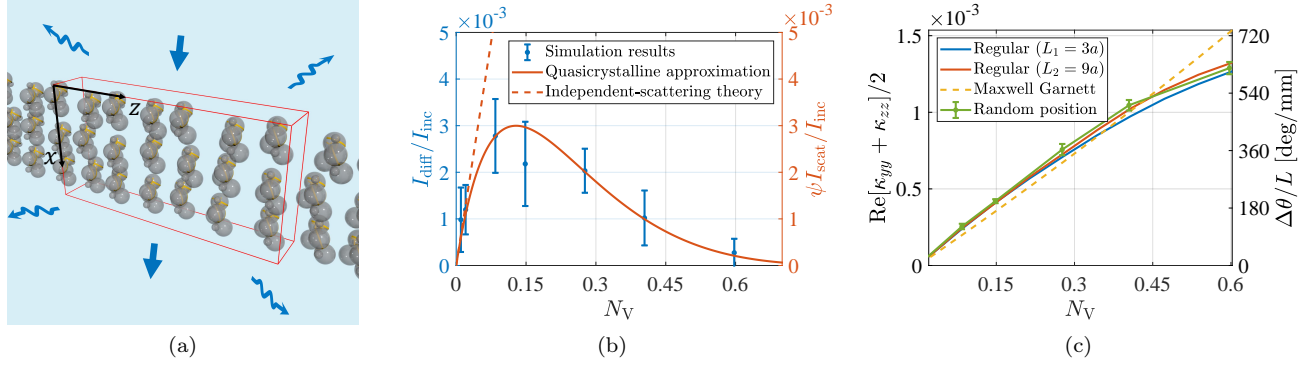


FIG. 2: (a) Calculation of light diffraction in a periodical water colloid metamaterial with random positions in the  $xz$ -plane of the chiral constituent meta-atoms. The unit cell is illustrated by the red box. The meta-atom distribution is periodical along the  $y$ - and  $z$ -directions. The figure depicts the scenario with volume fraction  $N_V = 0.6$ . (b) Comparison of the intensity loss in form of the simulated diffraction loss (in periodic arrangement shown in (a)) and scattering loss calculated using analytical fitting models (based on independent-scattering theory and QCA theory). The vertical blue bars denote the standard deviation of the values obtained in electromagnetic simulations. (c) In-plane chirality parameter  $(\kappa_{yy} + \kappa_{zz})/2$  and specific optical rotation of the designed metamaterial versus the volume fraction. All the data corresponds to the operational frequency of 400 THz.

to calculate the figure of merit, we consider the attenuation coefficient  $\beta = 2k_0\text{Im}(n)$  of the colloid metamaterial which shows how much light is attenuated over propagation distance  $L$ , i.e.  $I(L) = I(0)e^{-\beta L}$ . As mentioned above, the primary origin of the attenuation is from incoherent light scattering, which arises from the irregular distribution of the constituent meta-atoms in the metamaterial (fluctuations of density of scatterers). The incoherent scattering occurs even in the situations when the average distance between the meta-atoms is much smaller than the wavelength and the medium can be considered as uniform [57].

According to the classical independent-scattering formulation of the radiative transfer theory, the total scattering in a colloid is proportional to the volume concentration of its constituent meta-atom [58–62]. Under this assumption, the scatterings from all the meta-atoms are uncorrelated and  $\beta_{\text{uncorr}}(N) = 2k_0\text{Im}(n) = N\sigma$ , where  $\sigma$  is the extinction cross section of individual meta-atom. However, as it was demonstrated in the early works of Twersky et al. [58, 63, 64], this assumption is accurate only for media with low volume fraction  $N_V$ . In dense colloids, there exist correlations in positions of the meta-atoms which lead to the modified attenuation coefficient:

$$\beta_{\text{corr}}(N, N_V) = N\sigma W(N_V) = 2k_0\text{Im}(n_{\text{corr}}), \quad (7)$$

where  $W(N_V) = (1 - N_V)^4/(1 + 2N_V)^2$  is the so-called packing factor for spherical-shape constituent meta-atoms [58] and  $\text{Im}(n_{\text{corr}}) = \text{Im}(n)W(N_V)$  is the effective refractive index of the colloid metamaterial whose imaginary part is scaled by the packing factor. The factor  $W(N_V)$  monotonically decreases with increasing volume fraction, leading to the fact that attenuation due to incoherent scattering in dense colloid metamaterials can be several orders of magnitude smaller than that predicted

by the independent-scattering theory. Such scattering reduction can be intuitively understood by increased regularity of the colloid due to the loss of available space for its constituent meta-atoms. Equation (7), which was sometimes referred to as the quasicrystalline approximation (QCA), was subsequently confirmed for dense media experimentally [59, 62] and numerically [61].

In our study, we exploit the effect of scattering loss reduction to design a chiral dielectric colloid metamaterial with high figure of merit  $|\kappa|/\text{Im}(n_{\text{corr}})$ . For our system, the maximum volume fraction of the colloid is approximately  $N_{V,\text{max}} = 0.63$ , which is the measured value of  $N_V$  for densely packed amorphous solids of identical spheres [65]. This volume fraction corresponds to that of the mean of the cubic and hexagonal packings. In order to analyze the attenuation coefficient  $\beta$  in our colloid metamaterial, we calculate diffraction intensity for light propagating in it along the  $x$ -axis over length  $L$  using full-wave simulations. We use periodic boundary conditions along the  $y$ - and  $z$  directions (the unit cell is shown by the red box in Fig. 2(a)). The unit-cell size was chosen to be large enough to allow for multiple diffraction orders in the simulation. The power in the non-zero diffraction orders provide a measure of the incoherent scattering loss in truly random systems. The simulated total diffracted intensity  $I_{\text{diff}}$  normalized by the incident intensity  $I_{\text{inc}}$  is plotted in Fig. 2(b) versus the volume fraction. For each of the seven discrete values of  $N_V$ , we performed simulations with five random spatial distributions of the chiral meta-atoms in the  $xz$ -plane (at this stage, positions along the  $y$ -axis and the orientations of the meta-atoms were fixed due to the small sample group size). Furthermore, we additionally plot in Fig. 2(b) the incoherent scattering intensity loss calculated based on two analytical fitting models. The first model is

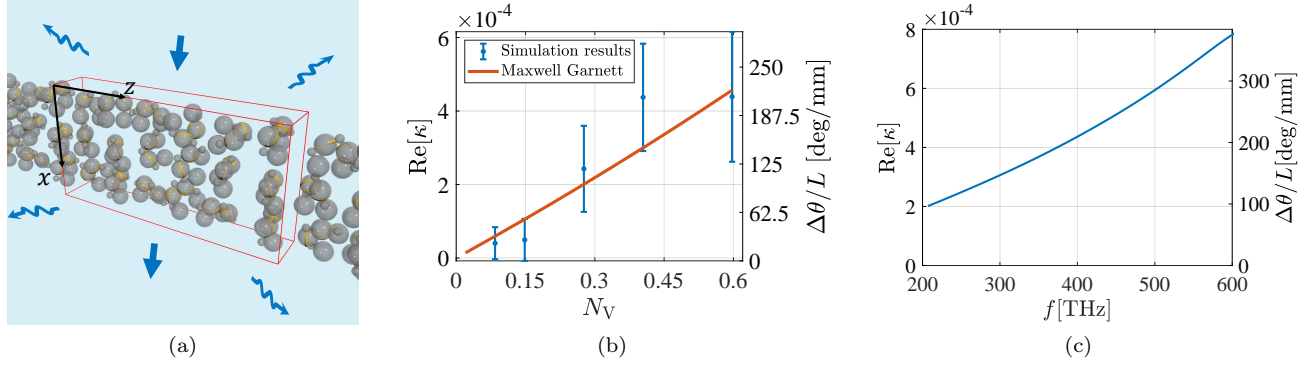


FIG. 3: (a) Calculation of light diffraction in a periodical water colloid with random orientations and positions (in the  $xz$ -plane) of the chiral meta-atoms. The unit cell is illustrated by the red box. The meta-atom distribution is periodical along the  $y$ - and  $z$ -directions. The figure depicts the scenario with volume fraction  $N_V = 0.6$ . (b) Intrinsic (isotropic) chirality parameter and specific rotation of the colloid versus the volume fraction. The plotted data corresponds to the operational frequency  $f = 400$  THz. (c) Frequency dispersion of the isotropic chirality parameter and specific optical rotation of the random colloid metamaterial with the volume fraction of meta-atoms  $N_V = 0.6$ .

based on the aforementioned QCA theory and implies  $I_{\text{scat}}/I_{\text{inc}} = [I(0) - I(L)]/I(0) = 1 - e^{-\beta_{\text{corr}}L} \approx \beta_{\text{corr}}L$ . We expect the ratios  $I_{\text{scat}}/I_{\text{inc}}$  and  $I_{\text{diff}}/I_{\text{inc}}$  to be proportional to one another with some unknown proportionality coefficient  $\psi$ . Substituting  $\beta_{\text{corr}}$  from (7), we chose  $\psi\sigma L = 7.4 \cdot 10^{-23} \text{ m}^3$  which ensures the best fitting for the simulated curve in Fig. 2(b). As is seen, the simulated diffraction loss follows the same dependence on  $N_V$  as the theoretical orange fitting curve predicted by the QCA theory. The corresponding scattering loss predicted by the independent-scattering theory is plotted by the orange dashed line. Summarizing, one can see that incoherent scattering in the designed colloid metamaterial is in fact suppressed by the factor  $1/W(N_V)$  in accordance with the QCA theory. Thus, for high concentrations of the meta-atoms in the colloid, the scattering loss decreases when the volume concentration increases.

In contrast to scattering loss, the chirality parameter of the semi-ordered colloid monotonically increases with  $N_V$ , as shown by the green curve in Fig. 2(c) (from full-wave simulations). Additionally, the figure depicts simulated chirality parameter extracted from transmission data for regular (without concentration fluctuations) dielectric colloid metamaterials with two thicknesses along the propagation direction  $L_1 = 3a$  and  $L_2 = 9a$ , where  $a$  is the interparticle distance. It is seen that the three curves are nearly the same, highlighting the fact that chirality is not significantly affected by the randomness in colloid metamaterials. Furthermore, the analytically calculated chirality parameter based on the polarizability tensors of individual meta-atoms and the Maxwell Garnett mixing rule is in good agreement with the simulated data, deviating from it only at high concentrations of the constituent meta-atoms.

Next, we analyze the chirality parameter versus the volume fractions for isotropic colloids whose constituent meta-atoms have random orientations in addition to ran-

dom positioning in the  $xz$ -plane, as shown in Fig. 3(a). The simulation setup is similar to that in the previous scenario. Figure 3(b) depicts the isotropic chirality parameter extracted from the transmission data along with the analytical results based on the Maxwell Garnett model and the data from Table (I). We have performed ten simulations with random meta-atom distribution for each of the five values of  $N_V$ . Although the standard deviation is considerably larger in this scenario, it clearly confirms that in the random colloid, the intrinsic chirality is preserved even for high concentrations. The right vertical axis in Fig. 3(b) shows the specific optical rotatory power calculated as  $\Delta\theta/L = \kappa\omega/c$ .

Figure 3(c) depicts the frequency dispersion of the isotropic chirality parameter in the random colloid metamaterial shown in Fig. 3(a) with the volume fraction of meta-atoms  $N_V = 0.6$ . The data were extracted using the full-wave simulations and theoretical formulation for chiral slabs [56, p. 83]. As is seen, in the frequency range from 200 THz to 600 THz, the colloid metamaterial is nonresonant, providing high isotropic chirality with very large bandwidth. At the higher frequencies, the meta-atoms sizes become comparable to the wavelength in water, and the colloid cannot be considered as a homogeneous metamaterial.

Table (II) compares different optical characteristics of the chiral colloids suitable for large-scale fabrication. As is seen, the dielectric colloid metamaterial presented in this work exhibits three orders of magnitude increase for the chirality parameter and figure of merit (expressed as  $|\kappa|/\text{Im}(n)$ ) compared to previous publications. Such striking improvement is due to the two factors: The absence of plasmonic losses and scattering loss reduction due to the high-density colloidal arrangement of the dielectric meta-atoms. It is also worth mentioning that the designed isotropic colloid metamaterial exhibits specific rotation more than two order of magnitude larger than

$\lambda$ [nm]	$N$ [ $\text{m}^{-3}$ ]	$ \text{tr}\{\bar{\alpha}_{\text{em}}\} /3$ [ $\text{m}^3$ ]	$ \kappa $	$\text{Im}(n_+ + n_-)/2$	FOM	Ref.
750	$6.0 \cdot 10^{14}$	$1.7 \cdot 10^{-22}$	$1.0 \cdot 10^{-7}$	$9.5 \cdot 10^{-6}$	0.01	[66]
549	$2.4 \cdot 10^{17}$	$6.3 \cdot 10^{-26}$	$1.5 \cdot 10^{-8}$	$1.5 \cdot 10^{-6}$	0.01	[29]
560	$1.8 \cdot 10^{17}$	$5.2 \cdot 10^{-27}$	$9.3 \cdot 10^{-10}$	–	–	[30]
750	$5.2 \cdot 10^{20}$	$7.9 \cdot 10^{-25}$	$4.3 \cdot 10^{-4}$	$4.1 \cdot 10^{-5}$	11.3	Our work

TABLE II: Comparison of optical characteristics of different chiral colloids.

that of natural substances like sugar [67], and even one order of magnitude larger than that in anisotropic alpha-quartz crystal [68].

In summary, we have designed a dielectric metamaterial consisting of a random colloid of specifically designed silicon nanoparticles which exhibits record-high isotropic chirality with significantly suppressed incoherent scattering. The suggested geometry of the chiral constituent meta-atoms favours large-scale mass production. This is in strong contrast with the previous designs of dielectric chiral metamaterials and colloids which either suffered from low writing speeds [69] or were suitable only for low colloid concentrations (such colloids were achieved by dispersing nanoparticles from a two-dimensional area into a bulk solution) [32, 33, 70]. It should be mentioned that although in this work, we concentrated on sub-wavelength dielectric meta-atoms, it is possible to

extend this study towards meta-atoms of larger sizes. In this case, the regime of strong Mie resonances can be achieved, which would further increase the isotropic chirality of the colloid by one or several orders of magnitude. The higher order multipole moments in isotropic samples do not contribute to chirality due to orientational averaging [16, p. 142, 227], and therefore, the theory presented in this paper can be still applied. Moreover, the QCA analysis demonstrated here can be extended to the case of meta-atoms with higher order multipole moments (see e.g. [71]).

This work was supported in part by the Finnish Foundation for Technology Promotion, by the U.S. National Science Foundation Grant No. (CBET-1641069), and by the Vannevar Bush Faculty Fellowship for U. S. Department of Defense (N00014-17-1-3030).

- 
- [1] C. M. Soukoulis and M. Wegener, “Past achievements and future challenges in the development of three-dimensional photonic metamaterials,” *Nature Photonics*, vol. 5, p. 523, Sept. 2011.
- [2] M. Albooyeh, S. Kruk, C. Menzel, C. Helgert, M. Kroll, A. Krysinski, M. Decker, D. N. Neshev, T. Pertsch, C. Etrich, C. Rockstuhl, S. A. Tretyakov, C. R. Simovski, and Y. S. Kivshar, “Resonant metasurfaces at oblique incidence: Interplay of order and disorder,” *Scientific Reports*, vol. 4, p. 04484, Mar. 2014.
- [3] P. Titum, N. H. Lindner, M. C. Rechtsman, and G. Refael, “Disorder-induced Floquet topological insulators,” *Physical Review Letters*, vol. 114, p. 056801, Feb. 2015.
- [4] M. A. Bandres, M. C. Rechtsman, and M. Segev, “Topological photonic quasicrystals: Fractal topological spectrum and protected transport,” *Physical Review X*, vol. 6, p. 011016, Feb. 2016.
- [5] A. Agarwala and V. B. Shenoy, “Topological insulators in amorphous systems,” *Physical Review Letters*, vol. 118, p. 236402, June 2017.
- [6] M. Xiao and S. Fan, “Photonic Chern insulator through homogenization of an array of particles,” *Physical Review B*, vol. 96, p. 100202, Sept. 2017.
- [7] C. Liu, M. V. Rybin, P. Mao, S. Zhang, and Y. Kivshar, “Disorder-immune photonics based on Mie-resonant dielectric metamaterials,” *Physical Review Letters*, vol. 123, p. 163901, Oct. 2019.
- [8] Y. Xia, B. Gates, and Z.-Y. Li, “Self-assembly approaches to three-dimensional photonic crystals,” *Advanced Materials*, vol. 13, no. 6, pp. 409–413, 2001.
- [9] S.-H. Kim, S. Y. Lee, S.-M. Yang, and G.-R. Yi, “Self-assembled colloidal structures for photonics,” *NPG Asia Materials*, vol. 3, pp. 25–33, Jan. 2011.
- [10] K. A. Arpin, M. D. Losego, A. N. Cloud, H. Ning, J. Mallek, N. P. Sergeant, L. Zhu, Z. Yu, B. Kalanyan, G. N. Parsons, G. S. Girolami, J. R. Abelson, S. Fan, and P. V. Braun, “Three-dimensional self-assembled photonic crystals with high temperature stability for thermal emission modification,” *Nature Communications*, vol. 4, pp. 1–8, Oct. 2013.
- [11] A. Ceconello, L. V. Besteiro, A. O. Govorov, and I. Willner, “Chiroplasmonic DNA-based nanostructures,” *Nature Reviews Materials*, vol. 2, pp. 1–19, July 2017.
- [12] N. Liu and T. Liedl, “DNA-assembled advanced plasmonic architectures,” *Chemical Reviews*, vol. 118, pp. 3032–3053, Mar. 2018.
- [13] A. Kuzyk, R. Jungmann, G. P. Acuna, and N. Liu, “DNA origami route for nanophotonics,” *ACS Photonics*, vol. 5, pp. 1151–1163, Apr. 2018.
- [14] A. Serdyukov, I. Semchenko, S. Tretyakov, and A. Sihvola, *Electromagnetics of Bi-Anisotropic Materials - Theory and Application*, vol. 11. Amsterdam: Gordon and Breach Science Publishers, 2001.
- [15] F. J. D. Arago, “Mémoire sur une modification remar-

- quable qu'éprouvent les rayons lumineux dans leur passage a travers certains corps diaphanes, et sur quelques autres nouveaux phénomènes d'optique," *Mémoires de la Classe des Sciences Mathématiques et Physiques de l'Institut Impérial de France: Part I*, pp. 93–134, 1811.
- [16] L. D. Barron, *Molecular Light Scattering and Optical Activity*. New York: Cambridge University Press, Oct. 2004.
- [17] M. Schäferling, *Chiral Nanophotonics: Chiral Optical Properties of Plasmonic Systems*. Cham: Springer International Publishing, 2017.
- [18] M. Hentschel, M. Schäferling, X. Duan, H. Giessen, and N. Liu, "Chiral plasmonics," *Science Advances*, vol. 3, p. e1602735, May 2017.
- [19] C. Caloz and A. Sihvola, "Electromagnetic chirality," *arXiv:1903.09087*, Apr. 2019.
- [20] K. F. Lindman, "Über eine durch ein isotropes system von spiralförmigen resonatoren erzeugte rotationspolarisation der elektromagnetischen wellen," *Annalen der Physik*, vol. 368, no. 23, pp. 621–644, 1920.
- [21] I. Tinoco and M. P. Freeman, "The optical activity of oriented copper helices. I. Experimental," *The Journal of Physical Chemistry*, vol. 61, pp. 1196–1200, Sept. 1957.
- [22] S. Ougier, I. Chenierie, and S. Bolioli, "Measurement method for chiral media," in *1992 22nd European Microwave Conference*, vol. 1, pp. 682–687, Sept. 1992.
- [23] F. Guérin, "Microwave chiral materials: A review of experimental studies and some results on composites with ferroelectric ceramic inclusions," *Progress In Electromagnetics Research*, vol. 9, pp. 219–263, 1994.
- [24] S. Tretyakov, I. Nefedov, A. Sihvola, S. Maslovski, and C. Simovski, "Waves and energy in chiral nihility," *Journal of Electromagnetic Waves and Applications*, vol. 17, pp. 695–706, Jan. 2003.
- [25] J. Kaschke and M. Wegener, "Optical and infrared helical metamaterials," *Nanophotonics*, vol. 5, no. 4, pp. 510–523, 2016.
- [26] Z. Wang, F. Cheng, T. Winsor, and Y. Liu, "Optical chiral metamaterials: A review of the fundamentals, fabrication methods and applications," *Nanotechnology*, vol. 27, p. 412001, Sept. 2016.
- [27] I. Fernandez-Corbaton, C. Rockstuhl, P. Ziemke, P. Gumbsch, A. Albiez, R. Schwaiger, T. Frenzel, M. Kadic, and M. Wegener, "New twists of 3D chiral metamaterials," *Advanced Materials*, vol. 31, no. 26, p. 1807742, 2019.
- [28] A. J. Mastroianni, S. A. Claridge, and A. P. Alivisatos, "Pyramidal and chiral groupings of gold nanocrystals assembled using DNA scaffolds," *Journal of the American Chemical Society*, vol. 131, pp. 8455–8459, June 2009.
- [29] A. Kuzyk, R. Schreiber, Z. Fan, G. Pardatscher, E.-M. Roller, A. Högele, F. C. Simmel, A. O. Govorov, and T. Liedl, "DNA-based self-assembly of chiral plasmonic nanostructures with tailored optical response," *Nature*, vol. 483, pp. 311–314, Mar. 2012.
- [30] X. Shen, A. Asenjo-Garcia, Q. Liu, Q. Jiang, F. J. Garcia de Abajo, N. Liu, and B. Ding, "Three-dimensional plasmonic chiral tetramers assembled by DNA origami," *Nano Letters*, vol. 13, pp. 2128–2133, May 2013.
- [31] C. Wu, N. Arju, G. Kelp, J. A. Fan, J. Dominguez, E. Gonzales, E. Tutuc, I. Brener, and G. Shvets, "Spectrally selective chiral silicon metasurfaces based on infrared Fano resonances," *Nature Communications*, vol. 5, p. 3892, May 2014.
- [32] R. Verre, L. Shao, N. O. Länk, P. Karpinski, A. B. Yankovich, T. J. Antosiewicz, E. Olsson, and M. Käll, "Metasurfaces and colloidal suspensions composed of 3d chiral Si nanoresonators," *Advanced Materials*, vol. 29, Aug. 2017.
- [33] H. J. Singh and A. Ghosh, "Large and tunable chiro-optical response with all dielectric helical nanomaterials," *ACS Photonics*, vol. 5, pp. 1977–1985, May 2018.
- [34] T.-H. Xiao, Z. Cheng, and K. Goda, "Giant optical activity in an all-dielectric spiral nanoflower," *Small*, vol. 14, no. 31, p. 1800485, 2018.
- [35] W. Gao, M. Lawrence, B. Yang, F. Liu, F. Fang, B. Béri, J. Li, and S. Zhang, "Topological photonic phase in chiral hyperbolic metamaterials," *Physical Review Letters*, vol. 114, p. 037402, Jan. 2015.
- [36] M. Xiao, Q. Lin, and S. Fan, "Hyperbolic Weyl point in reciprocal chiral metamaterials," *Physical Review Letters*, vol. 117, p. 057401, July 2016.
- [37] M. L. Solomon, J. Hu, M. Lawrence, A. García-Etxarri, and J. A. Dionne, "Enantiospecific optical enhancement of chiral sensing and separation with dielectric metasurfaces," *ACS Photonics*, vol. 6, pp. 43–49, Jan. 2019.
- [38] J. B. Pendry, "A chiral route to negative refraction," *Science*, vol. 306, pp. 1353–1355, Nov. 2004.
- [39] V. S. Asadchy, I. A. Faniayeu, Y. Ra'di, and S. A. Tretyakov, "Determining polarizability tensors for an arbitrary small electromagnetic scatterer," *Photonics and Nanostructures - Fundamentals and Applications*, vol. 12, pp. 298–304, Aug. 2014.
- [40] J. D. Jackson, *Classical Electrodynamics*. John Wiley Sons, Inc., 1999.
- [41] C. Schinke, P. Christian Peest, J. Schmidt, R. Brendel, K. Bothe, M. R. Vogt, I. Kröger, S. Winter, A. Schirmacher, S. Lim, H. T. Nguyen, and D. MacDonald, "Uncertainty analysis for the coefficient of band-to-band absorption of crystalline silicon," *AIP Advances*, vol. 5, p. 067168, June 2015.
- [42] D. G. Baranov, D. A. Zuev, S. I. Lepeshov, O. V. Kotov, A. E. Krasnok, A. B. Evlyukhin, and B. N. Chichkov, "All-dielectric nanophotonics: The quest for better materials and fabrication techniques," *Optica*, vol. 4, pp. 814–825, July 2017.
- [43] R. Fenollosa, F. Meseguer, and M. Tymczenko, "Silicon colloids: From microcavities to photonic sponges," *Advanced Materials*, vol. 20, no. 1, pp. 95–98, 2008.
- [44] X. Li, A. Pyatenko, Y. Shimizu, H. Wang, K. Koga, and N. Koshizaki, "Fabrication of crystalline silicon spheres by selective laser heating in liquid medium," *Langmuir*, vol. 27, pp. 5076–5080, Apr. 2011.
- [45] L. Shi, J. T. Harris, R. Fenollosa, I. Rodriguez, X. Lu, B. A. Korgel, and F. Meseguer, "Monodisperse silicon nanocavities and photonic crystals with magnetic response in the optical region," *Nature Communications*, vol. 4, pp. 1–7, May 2013.
- [46] M. Y. B. Zion, X. He, C. C. Maass, R. Sha, N. C. Seeman, and P. M. Chaikin, "Self-assembled three-dimensional chiral colloidal architecture," *Science*, vol. 358, pp. 633–636, Nov. 2017.
- [47] A. Fu, C. M. Micheel, J. Cha, H. Chang, H. Yang, and A. P. Alivisatos, "Discrete nanostructures of quantum dots/Au with DNA," *Journal of the American Chemical Society*, vol. 126, pp. 10832–10833, Sept. 2004.
- [48] W. Yan, L. Xu, C. Xu, W. Ma, H. Kuang, L. Wang, and N. A. Kotov, "Self-assembly of chiral nanoparticle pyramids with strong R/S optical activity," *Journal of the*

- American Chemical Society*, vol. 134, pp. 15114–15121, Sept. 2012.
- [49] F. Ma, S. Wang, D. T. Wu, and N. Wu, “Electric-field-induced assembly and propulsion of chiral colloidal clusters,” *Proceedings of the National Academy of Sciences*, vol. 112, pp. 6307–6312, May 2015.
- [50] D. Zerrouki, J. Baudry, D. Pine, P. Chaikin, and J. Bibette, “Chiral colloidal clusters,” *Nature*, vol. 455, pp. 380–382, Sept. 2008.
- [51] F. Freire, J. M. Seco, E. Quiñoá, and R. Riguera, “Nanospheres with tunable size and chirality from helical polymer-metal complexes,” *Journal of the American Chemical Society*, vol. 134, pp. 19374–19383, Nov. 2012.
- [52] J. A. Fan, C. Wu, K. Bao, J. Bao, R. Bardhan, N. J. Halas, V. N. Manoharan, P. Nordlander, G. Shvets, and F. Capasso, “Self-assembled plasmonic nanoparticle clusters,” *Science*, vol. 328, pp. 1135–1138, May 2010.
- [53] Y. Wang, Y. Wang, X. Zheng, t. Ducrot, M.-G. Lee, G.-R. Yi, M. Weck, and D. J. Pine, “Synthetic strategies toward DNA-coated colloids that crystallize,” *Journal of the American Chemical Society*, vol. 137, pp. 10760–10766, Aug. 2015.
- [54] A. I. Kuznetsov, A. E. Miroschnichenko, M. L. Brongersma, Y. S. Kivshar, and B. Luk’yanchuk, “Optically resonant dielectric nanostructures,” *Science*, vol. 354, p. aag2472, Nov. 2016.
- [55] V. S. Asadchy and S. A. Tretyakov, “Modular analysis of arbitrary dipolar scatterers,” *Physical Review Applied*, vol. 12, p. 024059, Aug. 2019.
- [56] I. Lindell, A. Sihvola, S. Tretyakov, and A. Viitanen, *Electromagnetic Waves in Chiral and Bi-Isotropic Media*. Boston: Artech House, 1994.
- [57] I. I. Sobel’man, “On the theory of light scattering in gases,” *Physics-Uspexhi*, vol. 45, no. 1, p. 75, 2002.
- [58] V. Twersky, “Transparency of pair-correlated, random distributions of small scatterers, with applications to the cornea,” *JOSA*, vol. 65, pp. 524–530, May 1975.
- [59] A. Ishiniaru and Y. Kuga, “Attenuation constant of a coherent field in a dense distribution of particles,” *JOSA*, vol. 72, pp. 1317–1320, Oct. 1982.
- [60] L. Tsang and J. A. Kong, “Effective propagation constants for coherent electromagnetic wave propagation in media embedded with dielectric scatterers,” *Journal of Applied Physics*, vol. 53, pp. 7162–7173, Nov. 1982.
- [61] L. Tsang, C. E. Mandt, and K. H. Ding, “Monte Carlo simulations of the extinction rate of dense media with randomly distributed dielectric spheres based on solution of Maxwell’s equations,” *Optics Letters*, vol. 17, pp. 314–316, Mar. 1992.
- [62] R. West, D. Gibbs, L. Tsang, and A. K. Fung, “Comparison of optical scattering experiments and the quasi-crystalline approximation for dense media,” *JOSA A*, vol. 11, pp. 1854–1858, June 1994.
- [63] S. Hawley, T. Kays, and V. Twersky, “Comparison of distribution functions from scattering data on different sets of spheres,” *IEEE Transactions on Antennas and Propagation*, vol. 15, pp. 118–135, Jan. 1967.
- [64] V. Twersky, “Acoustic bulk parameters in distributions of pair-correlated scatterers,” *The Journal of the Acoustical Society of America*, vol. 64, pp. 1710–1719, Dec. 1978.
- [65] G. D. Scott, “Packing of spheres: Packing of equal spheres,” *Nature*, vol. 188, pp. 908–909, Dec. 1960.
- [66] K. M. McPeak, C. D. van Engers, M. Blome, J. H. Park, S. Burger, M. A. Gosálvez, A. Faridi, Y. R. Ries, A. Sahu, and D. J. Norris, “Complex chiral colloids and surfaces via high-index off-cut silicon,” *Nano Letters*, vol. 14, pp. 2934–2940, May 2014.
- [67] D. R. Lide, *CRC Handbook of Chemistry and Physics*. CRC Press, June 2004.
- [68] W. Kaminsky, “Experimental and phenomenological aspects of circular birefringence and related properties in transparent crystals,” *Reports on Progress in Physics*, vol. 63, pp. 1575–1640, Sept. 2000.
- [69] M. Thiel, M. S. Rill, G. v. Freymann, and M. Wegener, “Three-dimensional bi-chiral photonic crystals,” *Advanced Materials*, vol. 21, no. 46, pp. 4680–4682, 2009.
- [70] L. Lin, S. Lepeshov, A. Krasnok, T. Jiang, X. Peng, B. A. Korgel, A. Alù, and Y. Zheng, “All-optical reconfigurable chiral meta-molecules,” *Materials Today*, vol. 25, pp. 10–20, May 2019.
- [71] L. Tsang, C.-T. Chen, A. T. C. Chang, J. Guo, and K.-H. Ding, “Dense media radiative transfer theory based on quasicrystalline approximation with applications to passive microwave remote sensing of snow,” *Radio Science*, vol. 35, pp. 731–749, May 2000.